scientific data

OPEN

DATA DESCRIPTOR

GNSS land subsidence observations along the northern coastline of Java, Indonesia

Susilo Susilo[1]✉, Rino Salman[2]✉, Wawan Hermawan[3], Risna Widyaningrum[3], Sidik Tri Wibowo[4], Yustisi Ardhitasari Lumban-Gaol[1], Irwan Meilano[5] & Sang-Ho Yun[2,6,7]

Land subsidence in cities along the northern coastline of Java has been at a worrying level. Monitoring efforts using geodetic data reveal that Jakarta, Pekalongan, Semarang, and Demak subside at least ~9x faster than the present-day rate of global sea level rise, which affects the cities' future urban viability. In this study, we publish a time series of the precise 3D displacements observed by twenty continuous Global Navigation Satellite System (GNSS) stations between 2010 and 2021. These are the first open-to-the-public and rigorously processed GNSS datasets that are useful for accurately quantifying land subsidence in the densely populated sinking cities in Java. The data also provides a way to tie other geodetic observations, such as Interferometric Synthetic Aperture Radar (InSAR), to a global reference frame in an attempt to build worldwide observations of coastal land subsidence.

Background & Summary

The northern coastline regions of Java have been soliciting the attention of many studies because a large portion of land in at least ten cities is subsiding[1–18] (Fig. 1). The subsiding land has been triggered by a wide range of natural and anthropogenic activities, such as the compaction of sediments in Pekalongan, Semarang, and Demak[19,20], gas extraction in Sidoarjo[16], and structural loadings in Jakarta[1]. In addition, excessive groundwater extraction is the most significant triggering factor due to the increasing demand and need for residential and industrial water supply[2,16,21–24]. In these cities, the impacts of land subsidence such as widespread coastal inundation and structural damage to buildings, have been significantly reducing the quality of the living environment[1,2,5,14,17,20,25–27]. In Jakarta, the capital city of Indonesia, land subsidence is so severely affecting the city's future urban viability[28] that government authorities are planning to move the capital to Borneo[29].

Monitoring efforts to study the spatial extent of land subsidence and its rates in these cities have been continuously made using land-based and space-borne techniques[1–4,6–11,15,16,27,30]. Out of the ten cities, land subsidence in Jakarta and Semarang has been the most intensively studied with a long monitoring history. In Jakarta, levelling surveys and campaign GNSS measurements between 1982 and 2010 estimate that the rates are from 1 to 28 cm/year[1]. A recent study using Sentinel-1 InSAR data between 2014 and 2020 estimates that the rates are from 1 to ~11 cm/year[7,8]. Different rates between the past and recent monitoring efforts have also been observed in Semarang: GNSS measurements between 1999 and 2011 estimate that the rates are from 14 to 19 cm/year[2], while a recent study using Sentinel-1 InSAR data between 2015 and 2020 reveals that the rates are from 2 to 3 cm/year[8].

Besides Jakarta and Semarang, land subsidence monitoring efforts using InSAR data in the remaining cities have been rapidly growing since 2013[3,4,6,9,11,16,31–33] thanks to the availability of open access SAR data from the Copernicus Sentinel-1 satellites operated by the European Space Agency. On the contrary, since 2013, the monitoring efforts using campaign GNSS measurements have been lacking; the latest measurements were in 2010 for Jakarta[1], in 2017 for Semarang[12], and in 2018 for Demak[10]. Even worse, no study reported GNSS-based

[1]National Agency for Research and Innovation (BRIN), Jakarta, Indonesia. [2]Earth Observatory of Singapore, Nanyang Technological University, Singapore, Singapore. [3]Center for Groundwater and Environmental Geology, Geological Agency, Bandung, Indonesia. [4]Geospatial Information Agency (BIG), Cibinong, Indonesia. [5] Faculty of Earth Sciences and Technology, Institute of Technology Bandung (ITB), Bandung, Indonesia. [6]Asian School of the Environment, Nanyang Technological University, Singapore, Singapore. [7]School of Electrical and Electronic Engineering, Nanyang Technological University, Singapore, Singapore. ✉e-mail: susilo.2@brin.go.id; rino@ntu.edu.sg

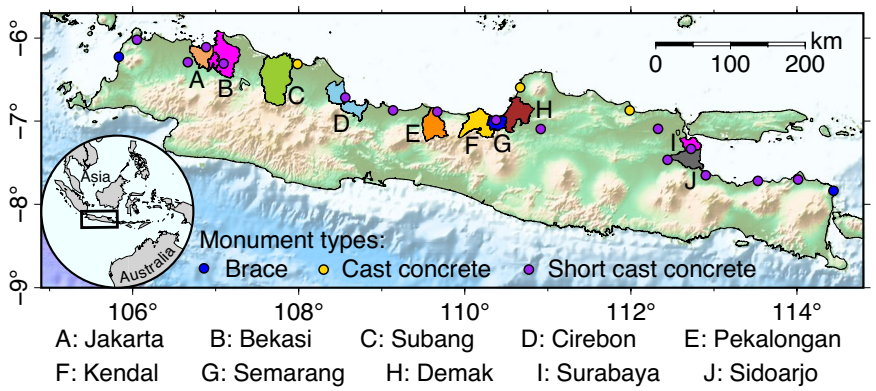

Fig. 1 Administrative boundaries of coastal cities along the northern coastline regions of Java that are known to experience land subsidence[1–18].

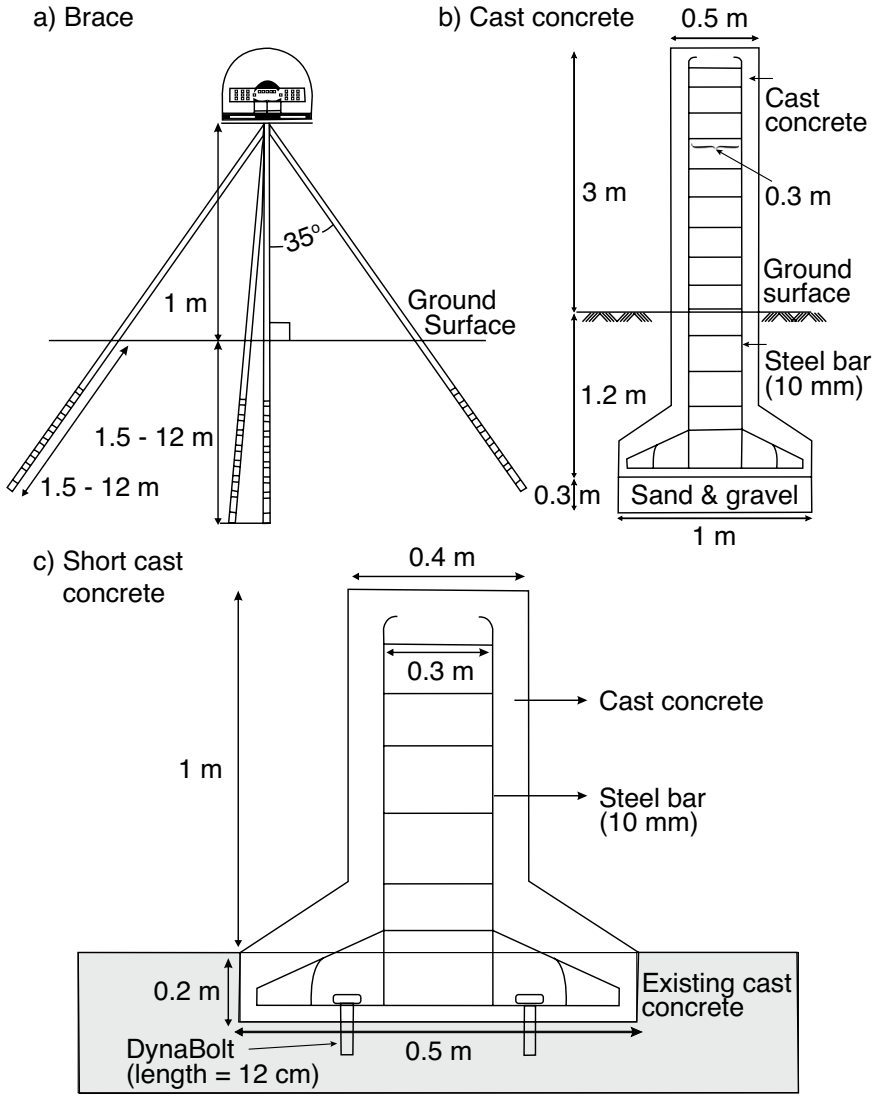

Fig. 2 Monument types of the BIG GNSS stations used in this study.

monitoring efforts in other cities that are known to experience land subsidence, such as Bekasi, Subang, Pekalongan, and Surabaya. This lack of GNSS-based monitoring efforts is worrying because the GNSS data is still needed for several reasons.

Site	Monument type	Receiver type	Antenna type	Data transmission	First observation
CPSR	BRACE	TRIMBLE ALLOY	LEIAT504	VPN	2010
CGON	SCC	TRIMBLE ALLOY	LEIAR20	VPN	2010
CTGR	SCC	TRIMBLE ALLOY	LEIAR25	VPN	2009
CJKT	SCC	TRIMBLE ALLOY	LEIAR20	VPN	2010
CBTU	SCC	LEICA GR10	LEIAR25	VPN	2010
CROL	CC	TRIMBLE ALLOY	LEIAR25	VPN	2010
CCIR	SCC	LEICA GR50	TPSCR.G3	VPN	2010
CTGL	SCC	LEICA GR50	LEIAR25	VPN	2010
CSEM	SCC	LEICA GR50	TPSCR.G3	VPN	2010
CJPR	CC	TRIMBLE ALLOY	HX-C6X601A	VPN	2010
CPKL	CC	LEICA GR50	LEIAR25	VPN	2010
CPWD	SCC	LEICA GR50	LEIAR20	VPN	2010
CTBN	CC	TPS NET-G3A	TPSCR.G3	VPN	2010
CLMG	SCC	LEICA GR50	TPSCR.G3	VPN	2010
CMJT	SCC	LEICA GR50	TPSCR.G3	VPN	2010
CSBY	SCC	LEICA GR50	TPSCR.G3	VPN	2010
CPAS	SCC	TPS NET-G3A	TPSCR.G3	VPN	2010
CPAI	SCC	TPS NET-G3A	TPSCR.G3	VPN	2010
CSIT	SCC	TPS NET-G3A	TPSCR.G3	VPN	2010
CBRN	BRACE	TRIMBLE ALLOY	LEIAT504	Offline	2008

Table 1. GNSS station specifications. CC: Cast Concrete; SCC: Short Cast Concrete.

1. Meteorology sensor 2. GPS receiver
3. Automatic battery charger 4. VPN modem
5. Battery

Fig. 3 Components of the BIG GNSS stations.

Site	Longitude (degree)	Latitude (degree)	Vertical velocity (mm/year)	Uncertainty (mm/year)
CPSR	105.834	−6.226	−1.0	0.052
CGON	106.052	−6.021	0.0	0.043
CTGR	106.664	−6.291	−2.9	0.049
CJKT	106.885	−6.110	−6.4	0.043
CBTU	107.096	−6.308	−0.5	0.044
CROL	107.985	−6.313	−15.9	0.045
CCIR	108.561	−6.716	−2.3	0.041
CTGL	109.136	−6.871	−12.5	0.043
CSEM	110.377	−6.987	−0.8	0.038
CJPR	110.667	−6.596	−2.7	0.056
CPKL	109.669	−6.887	−107.0	0.202
CPWD	110.914	−7.096	−1.1	0.044
CTBN	111.986	−6.872	0.4	0.042
CLMG	112.327	−7.093	−4.9	0.041
CMJT	112.442	−7.466	−1.3	0.042
CSBY	112.724	−7.334	−2.2	0.039
CPAS	112.901	−7.651	−1.4	0.033
CPAI	113.530	−7.719	−3.5	0.039
CSIT	114.013	−7.703	0.1	0.041
CBRN	114.440	−7.838	−2.1	0.082

Table 2. Vertical velocity recorded by the BIG GNSS stations along the northern coastline regions of Java.

First, although InSAR observations provide all-weather and day-night monitoring capacity at high spatial coverage and resolution[34,35], InSAR accuracy may still be degraded by various noise sources such as atmospheric phase delays, satellite orbit uncertainty, and unwrapping errors[36,37]. The degraded accuracy may mislead the interpretation of the subsidence rate. Incorporating independent data from GNSS measurements can help mitigate the false interpretation[38,39]. Second, InSAR velocity maps are relative to a reference point within the SAR data footprints. In areas where GNSS data is not available, a common approach to select a reference point is by assuming a certain area to be stable. However, this approach is subjective and may result in varying InSAR velocity maps across different studies. For example, Tay *et al.*[7] showed that a location on the northern coastline of Jakarta subsides ~7x faster than that reported by Wu *et al.*[8]. One possible explanation for this discrepancy is the use of different reference points. Therefore, GNSS data is necessary to provide a priori information for selecting a stable reference point. Third, InSAR velocity maps are 1D measurements of surface deformations in the radar line-of-sight direction of SAR satellites[34,35]. In the case of land subsidence monitoring where vertical motions are of interest, other data sets such as GNSS observations are needed to isolate the vertical motions precisely (e.g.[40–43]). Fourth, Shirzaei *et al.*[44] suggest the need for incorporating geocentric global reference frame vertical land motion (VLM) into global mean sea level (GMSL) studies. Geocentric is the natural for a global frame. Therefore, GMSL studies relative to this frame will allow us to determine whether a given location is rising or falling relative to the centre of the Earth. The InSAR-based VLM measurements are ideal for this purpose because InSAR data provide global coverage observations. However, the main challenge is that InSAR results are provided in a local reference frame. Thus, establishing worldwide InSAR-based VLM measurements needs GNSS data to tie the VLM measurements into a global reference frame[44]. In this study, we publish a time series of 3D displacements observed at twenty continuous GNSS stations between 2010 and 2021 along the northern coastline regions of Java (Fig. 1). The data may potentially be used for all the purposes mentioned above.

Observation specifications. We obtain the Receiver Independent Exchange (RINEX) GNSS data from the Geospatial Information Agency of Indonesia (BIG) which has been establishing and maintaining continuous GNSS stations in the country since 1996. Most stations are located on the national telecommunication company network. The stations use different monument types (Fig. 2) and record data continuously at one sample per second using high-precision L1/L2 geodetic type receivers and standard Choke Ring antennas (Table 1). In addition, the stations also have meteorological instrument systems, an automatic battery charger that connects to the national power network, and a cell modem (Fig. 3) that will stream the recorded raw data via a secure TCP/IP connection to BIG's data processing centre in Cibinong, West Java up to one-hour latency.

Methods

We processed the RINEX GNSS data and obtained a time series of GNSS station coordinates using the GPS at MIT/Global Kalman filtering (GAMIT/GLOBK) software package version 10.71[45–47]. Our GPS processing consisted of two steps[48,49]. In the first step, we used double-differencing methods in the GAMIT software to estimate daily station positions, atmospheric parameters, satellite orbits, and earth orientation parameters from ionosphere-free linear combination GPS phase observations. During this step, we fixed the satellite orbit parameters to the IGS final orbits and applied a second-order ionospheric correction using IGS final ionospheric products. We set the computation parameters to the default GAMIT setting, except for the atmospheric

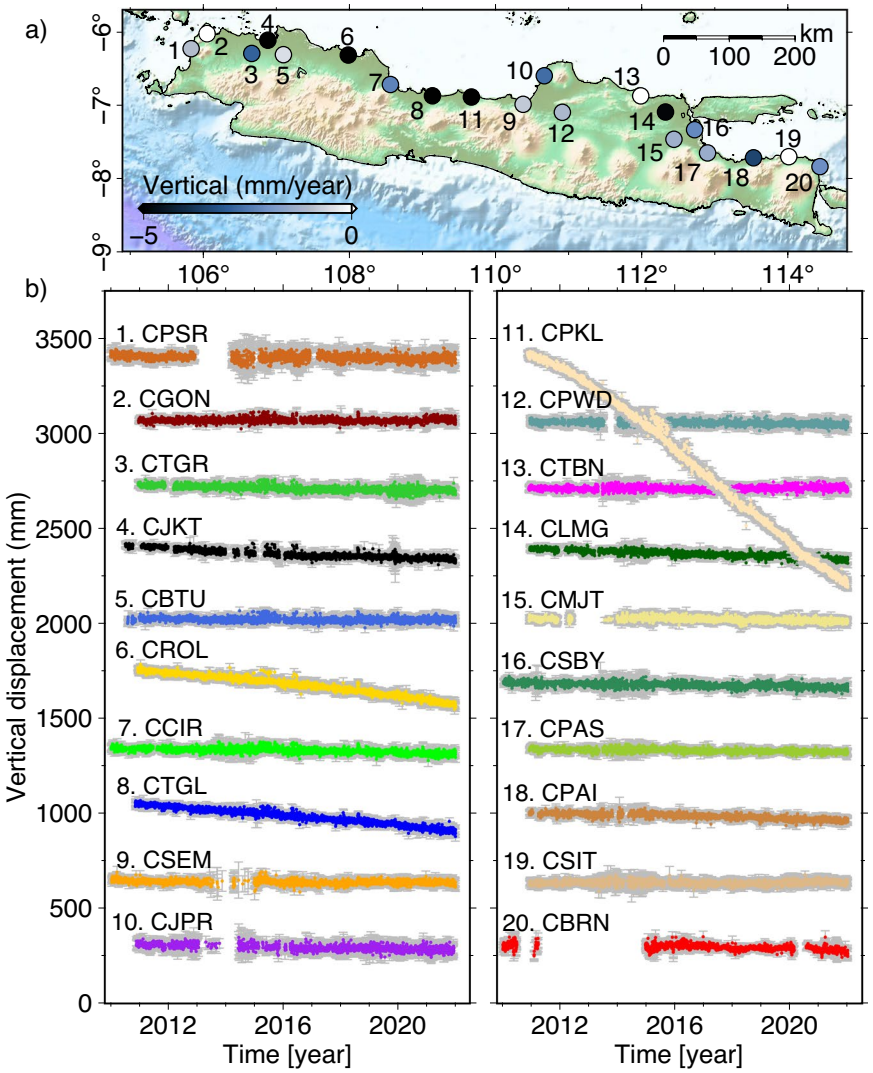

Fig. 4 Vertical component of the twenty BIG GNSS stations. (**a**) Negative vertical velocities are likely related to land subsidence. (**b**) Daily time series of the GNSS vertical component from 2010 to 2021.

delay parameters, which were modeled and estimated every hour using the Vienna Mapping Function[50]. We corrected the station displacements due to ocean tides using the most recent global ocean tide model, Finite Element Solution 2004[51]. To adjust the effect of solar and solid-earth tides, we applied the International Earth Rotation and Reference System Service 2010 standard model[52] and the atmospheric pressure loading model corrections[53]. Finally, we included GPS data from 12 International GNSS Services (IGS) stations (ALIC, BAKO, COCO, DARW, DGAR, GUAM, HYDE, IISC, LHAZ, PIMO, XMIS, YARR) in our daily processing to integrate our local network into the ITRF2014 reference frame[54].

In the second step, we used the GLOBK software to combine our daily solutions with the global GPS solutions provided by the MIT analysis centre. During this step, we aligned our combined solutions with the ITRF2014 reference frame[54] by minimising the position differences of eight selected sites[55], using a priori values defined by the IGb14 realisation of ITRF2014[54]. To accomplish this position difference minimation, we calculated six Helmert transformation parameters (three translations and three rotations) of eight selected reference sites: YARR in Australia, MAW1 and DAV1 in Antarctica, STJO and FLIN in North America, WSRT, ONSA, and NOT1 in Europe[55]. These sites were selected because they are less affected by earthquake deformations and hydrological loading[55]. Lastly, we generated daily time series coordinates for all the GNSS stations with respect to IGb14 realisation of ITRF2014[54].

Data Records

The processing results are a time series of 3D displacements from 2010 to 2021, relative to the ITRF2014. Most stations record negative velocities in the vertical component and are likely related to land subsidence (Table 2 and Fig. 4). The time series of the 3D displacements that include horizontal motions can be found in this repository: https://doi.org/10.5281/zenodo.7775016[56].

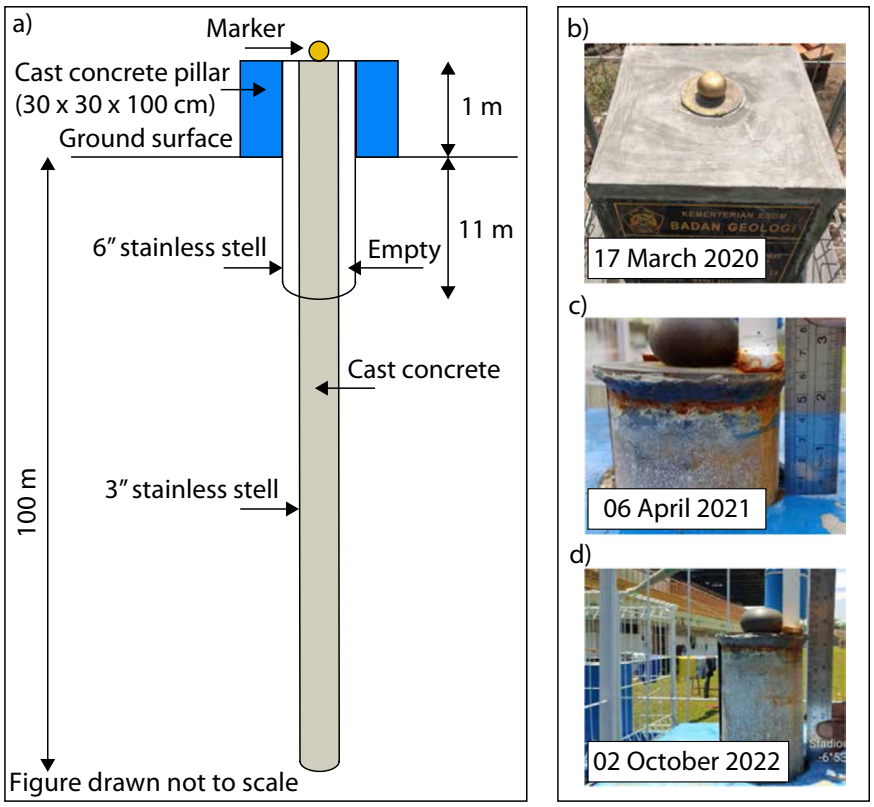

Fig. 5 A deep pile benchmark to measure land subsidence in Pekalongan. (**a**) A schematic design of the deep pile benchmark. (**b**) The newly installed benchmark. (**c**) The benchmark measures 60 ± 1 mm land subsidence by 06 April 2021. (**d**) The benchmark measures 140 ± 1 mm land subsidence by 02 October 2022, meaning that 80 ± 1 mm land subsidence occurs within ~1.5 years.

Technical Validation

Bad environments (e.g., buildings and trees) that degrade the sky view of the GNSS antenna will reflect and refract satellite signals before arriving at the antenna[57]. The reflected and refracted signals are called multipath signals which will introduce carrier phase measurement errors and subsequently lead to a positioning error[58]. A simple approach to inspect the environments surrounding the antenna is by plotting the signal-to-noise ratio (SNR) values measured by the GNSS receivers[59]. The SNR, like the carrier phase measurement, is also impacted directly by multipath signals and hence can therefore be used as a proxy to assess the environments surrounding the GNSS antenna[59,60]. Low SNR values indicate a large tracking error[59], meaning that multipath objects are present. We plot the SNR values using the L1 data recordings only. We do not use the L2 data due to its encrypted C/A code and the lack of civilian access to the P-code which affects the L2 SNR reliability[59]. We plot the SNR values as a function of azimuth and elevation angle, both in the time series and sky plot (Figure S1). The SNR plot shows that all the stations have SNR values greater than 30 decibels, indicating good environments surrounding the GNSS stations hence the negative velocities in the vertical component are robust.

In addition to SNR analysis, we use independent observation measured by a deep pile benchmark to validate the negative velocity at the GNSS CPKL station in Pekalongan (Table 2 and Fig. 4). The benchmark (Fig. 5) was installed by the centre for groundwater and environmental geology, Indonesia's geological agency, on 17 March 2020 ~500 m northeast of the GNSS CPKL station. The benchmark measurements between 06 April 2021 and 02 October 2022 estimate that ~80 ± 1 mm land subsidence occurs within ~1.5 years (Fig. 5c,d). Unfortunately, we cannot make a one-to-one comparison between this result and the amplitude of land subsidence measured at the GNSS CPKL station due to two reasons: 1) the benchmark and the GNSS CPKL station are ~500 m apart, 2) our GNSS data ended in 2021. Nevertheless, the benchmark measurements are still important in the sense that Pekalongan city is experiencing severe land subsidence.

Code availability

The GAMIT/GLOBK software we used to process the GNSS data is available at http://geoweb.mit.edu/gg/. The scripts we used to do the SNR analysis are available at https://github.com/ericlindsey/gnss-snr-skyplot.

Received: 27 January 2023; Accepted: 30 May 2023;
Published online: 01 July 2023

References

1. Abidin, H. Z. *et al*. Land subsidence of Jakarta (Indonesia) and its relation with urban development. *Nat. Hazards* **59** (2011).
2. Abidin, H. Z., Andreas, H., Gumilar, I., Sidiq, T. P. & Fukuda, Y. Land subsidence in coastal city of Semarang (Indonesia): Characteristics, impacts and causes. *Geomatics, Nat. Hazards Risk* **4** (2013).
3. Mochammad, M. & Saepuloh, A. Analyses of surface deformation with SBAR InSAR method and its relationship with aquifer occurrence in Surabaya City, East Java, Indonesia. in *IOP Conference Series: Earth and Environmental Science* vol. 71 (2017).
4. Parwata, I., Ogawara, K., Tanaka, T. & Osawa, T. Land Subsidence Monitoring From ALOS/PALSAR Data By Using D-InSAR Technique In Semarang City, Indonesia. *Int. J. Environ. Geosci.* **3**, 1–9 (2019).
5. Husnayaen *et al*. Physical assessment of coastal vulnerability under enhanced land subsidence in Semarang, Indonesia, using multi-sensor satellite data. *Adv. Sp. Res.* **61** (2018).
6. Sidiq, T. P. *et al*. Land Subsidence of Java North Coast Observed by SAR Interferometry. in *IOP Conference Series: Earth and Environmental Science* vol. 873 (2021).
7. Tay, C. *et al*. Sea-level rise from land subsidence in major coastal cities. *Nat. Sustain.* **5**, 1049–1057 (2022).
8. Wu, P. C., Wei, M. & D'Hondt, S. Subsidence in Coastal Cities Throughout the World Observed by InSAR. *Geophys. Res. Lett*. **49** (2022).
9. Yastika, P. E., Shimizu, N. & Abidin, H. Z. Monitoring of long-term land subsidence from 2003 to 2017 in coastal area of Semarang, Indonesia by SBAS DInSAR analyses using Envisat-ASAR, ALOS-PALSAR, and Sentinel-1A SAR data. *Adv. Sp. Res.* **63** (2019).
10. Yuwono, B. D., Subiyanto, S., Pratomo, A. S. & Najib, N. Time series of land subsidence rate on coastal demak using gnss cors udip and dinsar. in *E3S Web of Conferences* vol. 94 (2019).
11. Aditiya, A., Takeuchi, W. & Aoki, Y. Land Subsidence Monitoring by InSAR Time Series Technique Derived from ALOS-2 PALSAR-2 over Surabaya City, Indonesia. in *IOP Conference Series: Earth and Environmental Science* vol. 98 (2017).
12. Andreas, H. *et al*. On the acceleration of land subsidence rate in Semarang City as detected from GPS surveys. in *E3S Web of Conferences* vol. 94 (2019).
13. Aoki, Y. & Sidiq, T. P. Ground deformation associated with the eruption of Lumpur Sidoarjo mud volcano, east Java, Indonesia. *J. Volcanol. Geotherm. Res*. 278–279 (2014).
14. Bott, L. M. *et al*. Land subsidence in Jakarta and Semarang Bay – The relationship between physical processes, risk perception, and household adaptation. *Ocean Coast. Manag.* **211** (2021).
15. Bramanto, B., Gumilar, I., Sidiq, T. P., Rahmawan, Y. A. & Abidin, H. Z. Geodetic evidence of land subsidence in Cirebon, Indonesia. *Remote Sens. Appl. Soc. Environ.* **30**, 100933 (2023).
16. Chaussard, E., Amelung, F., Abidin, H. & Hong, S. H. Sinking cities in Indonesia: ALOS PALSAR detects rapid subsidence due to groundwater and gas extraction. *Remote Sens. Environ*. **128** (2013).
17. Gumilar, I. *et al*. Mapping And Evaluating The Impact Of Land Subsidence In Semarang (Indonesia). *Indones. J. Geospasial* **2**, 26–41 (2013).
18. Lubis, A. M., Sato, T., Tomiyama, N., Isezaki, N. & Yamanokuchi, T. Ground subsidence in Semarang-Indonesia investigated by ALOS-PALSAR satellite SAR interferometry. *J. Asian Earth Sci*. **40** (2011).
19. Sarah, D., Hutasoit, L. M., Delinom, R. M., Sadisun, I. A. & Wirabuana, T. A physical study of the effect of groundwater salinity on the compressibility of the semarang-demakaquitard, Java Island. *Geosci*. **8** (2018).
20. Sarah, D., Soebowo, E. & Satriyo, N. A. Review of the land subsidence hazard in pekalongan delta, central java: Insights from the subsurface. *Rud. Geol. Naft. Zb*. **36** (2021).
21. Bucx, T. H. M., Van Ruiten, C. J. M., Erkens, G. & De Lange, G. An integrated assessment framework for land subsidence in delta cities. in *Proceedings of the International Association of Hydrological Sciences* vol. 372 (2015).
22. Delinom, R. M. *et al*. The contribution of human activities to subsurface environment degradation in Greater Jakarta Area, Indonesia. *Sci. Total Environ*. **407** (2009).
23. Zoysa, R. S. D *et al*. The 'wickedness' of governing land subsidence: Policy perspectives from urban southeast Asia. *PLoS ONE* **16**, https://doi.org/10.1371/journal.pone.0250208 (2021).
24. Yan, X. *et al*. Advances and Practices on the Research, Prevention and Control of Land Subsidence in Coastal Cities. *Acta Geol. Sin. (English Ed*. **94** (2020).
25. Andreas, H., Pradipta, D., Abidin, H. Z. & Sarsito, D. A. Early pictures of global climate change impact to the coastal area (north west of demak central Java Indonesia). in *AIP Conference Proceedings* vol. 1857 (2017).
26. Andreas, H., Zainal Abidin, H., Pradipta, D., Anggreni Sarsito, D. & Gumilar, I. Insight look the subsidence impact to infrastructures in Jakarta and Semarang area; Key for adaptation and mitigation. in *MATEC Web of Conferences* vol. 147 (2018).
27. Andreas, H., Abidin, H. Z., Sarsito, D. A. & Pradipta, D. Adaptation of 'early climate change disaster' to the northern coast of Java Island Indonesia. *Eng. J.* **22** (2018).
28. Takagi, H., Esteban, M., Mikami, T. & Fujii, D. Projection of coastal floods in 2050 Jakarta. *Urban Clim*. **17** (2016).
29. Kompas. Presiden Jokowi ungkap alasan mengapa ibu kota RI harus pindah. https://nasional.kompas.com/read/2019/08/26/13475951/presiden-jokowi-ungkap-alasan-mengapa-ibu-kota-ri-harus-pindah (2019).
30. Abidin, H. Z., Andreas, H., Djaja, R., Darmawan, D. & Gamal, M. Land subsidence characteristics of Jakarta between 1997 and 2005, as estimated using GPS surveys. *GPS Solut*. **12** (2008).
31. Anjasmara, I. M., Mauradhia, A. & Susilo. Surface deformation and earthquake potential in Surabaya from GPS campaigns data. in *IOP Conference Series: Earth and Environmental Science* vol. 389 (2019).
32. Hakim, W. L., Achmad, A. R., Eom, J. & Lee, C. W. Land Subsidence Measurement of Jakarta Coastal Area Using Time Series Interferometry with Sentinel-1 SAR Data. *J. Coast. Res*. **102** (2020).
33. Zaenudin, A., Darmawan, I. G. B., Armijon, Minardi, S. & Haerudin, N. Land subsidence analysis in Bandar Lampung City based on InSAR. in *Journal of Physics: Conference Series* vol. 1080 (2018).
34. Burgmann, R., Rosen, P. A. & Fielding, E. J. Synthetic aperture radar interferometry to measure earth's surface topography and its deformation. *Annu. Rev. Earth Planet. Sci*. **28** (2000).
35. Simons, M. & Rosen, P. A. Interferometric Synthetic Aperture Radar Geodesy. in *Treatise on Geophysics: Second Edition* vol. 3 (2015).
36. Neely, W. R., Borsa, A. A. & Silverii, F. GInSAR: A cGPS Correction for Enhanced InSAR Time Series. *IEEE Trans. Geosci. Remote Sens*. **58** (2020).
37. Zebker, H. A., Rosen, P. A. & Hensley, S. Atmospheric effects in interferometric synthetic aperture radar surface deformation and topographic maps. *J. Geophys. Res. Solid Earth* **102** (1997).
38. Kanno, A. & Tanaka, Y. Modified lyzenga's method for estimating generalized coefficients of satellite-based predictor of shallow water depth. *IEEE Geosci. Remote Sens. Lett.* **9**, 715–719 (2012).
39. Yalvac, S. Validating InSAR-SBAS results by means of different GNSS analysis techniques in medium- and high-grade deformation areas. *Environ. Monit. Assess*. **192** (2020).
40. Hussain, E. *et al*. Geodetic observations of postseismic creep in the decade after the 1999 Izmit earthquake, Turkey: Implications for a shallow slip deficit. *J. Geophys. Res. Solid Earth* **121** (2016).
41. Tong, X., Sandwell, D. T. & Smith-Konter, B. High-resolution interseismic velocity data along the San Andreas Fault from GPS and InSAR. *J. Geophys. Res. Solid Earth* **118** (2013).
42. Shen, Z. K. & Liu, Z. Integration of GPS and InSAR Data for Resolving 3-Dimensional Crustal Deformation. *Earth Sp. Sci*. **7** (2020).

43. Xu, X., Sandwell, D. T., Klein, E. & Bock, Y. Integrated Sentinel-1 InSAR and GNSS Time-Series Along the San Andreas Fault System. *J. Geophys. Res. Solid Earth* **126** (2021).
44. Shirzaei, M. *et al*. Measuring, modelling and projecting coastal land subsidence. *Nature Reviews Earth and Environment* **2**, https://doi.org/10.1038/s43017-020-00115-x (2021).
45. Herring, T. A., King, R. W., Floyd, M. A. & McClusky, S. C. GLOBK Reference Manual. Global Kalman filter VLBI and GPS analysis program Release 10.6. 1–95 (2015).
46. Herring, T. A., King, R. W., Floyd, M. A., Mcclusky, S. C. & Sciences, P. Introduction to GAMIT/GLOBK Release 10.7. 1–168 (2018).
47. Herring, T. A., King, R. W., Floyd, M. A. & Mcclusky, S. C. GAMIT Reference Manual. GPS Analysis at MIT Release 10.7. 1–168 (2018).
48. Reilinger, R. *et al*. GPS constraints on continental deformation in the Africa-Arabia-Eurasia continental collision zone and implications for the dynamics of plate interactions. *J. Geophys. Res. Solid Earth* **111** (2006).
49. Koulali, A. *et al*. New Insights into the present-day kinematics of the central and western Papua New Guinea from GPS. *Geophys. J. Int*. **202** (2015).
50. Boehm, J., Werl, B. & Schuh, H. Troposphere mapping functions for GPS and very long baseline interferometry from European Centre for Medium-Range Weather Forecasts operational analysis data. *J. Geophys. Res. Solid Earth* **111** (2006).
51. Lyard, F., Lefevre, F., Letellier, T. & Francis, O. Modelling the global ocean tides: Modern insights from FES2004. *Ocean Dyn*. **56** (2006).
52. Petit, G. & Luzum, B. IERS Conventions (2010),IERS Technical Note 36. *Verlagdes Bundesamts für Kartographie und Geodäsie* (2010).
53. Tregoning, P. & van Dam, T. Atmospheric pressure loading corrections applied to GPS data at the observation level. *Geophys. Res. Lett*. **32** (2005).
54. Altamimi, Z., Rebischung, P., Métivier, L. & Collilieux, X. ITRF2014: A new release of the International Terrestrial Reference Frame modeling nonlinear station motions. *J. Geophys. Res. Solid Earth* **121** (2016).
55. Tregoning, P. *et al*. A decade of horizontal deformation from great earthquakes. *J. Geophys. Res. Solid Earth* **118** (2013).
56. Susilo, S. *et al*. The GNSS time series along the northern coastline of Java, Indonesia. *Zenodo* https://doi.org/10.5281/zenodo.7775016 (2023).
57. Blewitt, G. GPS and Space-Based Geodetic Methods. in *Treatise on Geophysics: Second Edition* vol. 3 (2015).
58. Bilich, A., Larson, K. M. & Axelrad, P. Modeling GPS phase multipath with SNR: Case study from the Salar de Uyuni, Boliva. *J. Geophys. Res. Solid Earth* **113** (2008).
59. Bilich, A., Larson, K. M. & Axelrad, P. Observations of Signal-to-Noise Ratios (SNR) at Geodetic GPS Site CASA: Implications for Phase Multipath. *Proc. Cent. Eur. Geodyn. Seismol*. **23** (2004).
60. Bilich, A., Axelrad, P. & Larson, K. M. Scientific utility of the signal-to-noise ratio (SNR) reported by geodetic GPS receivers. in *20th International Technical Meeting of the Satellite Division of The Institute of Navigation 2007 ION GNSS 2007* vol. 2 (2007).

Acknowledgements

We thank BIG for providing the RINEX GNSS data. Part of this research is supported by the Earth Observatory of Singapore (EOS) via its funding from the National Research Foundation Singapore and the Singapore Ministry of Education under the Research Centres of Excellence Initiative, the Ministry of Education Singapore under its Academic Research Fund Tier 3 MOE-MOET32021-0002 Award, and National Environment Agency Singapore under the National Sea Level Programme Funding Initiative (Award No. USS-IF-2020-5). I.M. is supported by RISPRO LPDP Indonesia Endowment Fund for Education S-303/LPDP.4/2022. S.S. and Y.A.L.G. are supported by the Disaster Seed Research Grant Program of the National Research and Innovation Agency of the Republic of Indonesia DIPA-124.01.1.690501/2023. This work comprises EOS contribution number 517.

Author contributions

S.S. and R.S. are the main contributor in conceptualisation, writing, formal analysis, and visualisation. S.S. carried out the GPS processing. Y.A.L.G. and S.Y. contributed to writing. W.H. and R.W. contributed to data validation measured by a deep pile benchmark. S.T.W. contributed to data curation. I.M. involved in discussions.

Competing interests

The authors declare no competing interests.

Additional information

Supplementary information The online version contains supplementary material available at https://doi.org/10.1038/s41597-023-02274-0.

Correspondence and requests for materials should be addressed to S.S. or R.S.